








Two-dimensional negative thermal expansion and ionic conductivity of a new glaserite-like ternary molybdate $\text{KZn}_{0.5}\text{Hf}_{0.5}(\text{MoO}_4)_2$

Evgeniy Kovtunets ^{a*} , Yunna Tushinova ^a , Tatyana Spiridonova ^a ,
Tsyrendyzhit Bazarova ^a , Alexandra Logvinova ^a , Alexandr Bogdanov ^b ,
Bair Bazarov ^a 

a: Laboratory of Oxide Systems, Baikal Institute of Nature Management (BINM SB RAS), Ulan-Ude 670047, Russia

b: Laboratory of Single Crystals Physics, Institute of Geochemistry (IGC SB RAS), Irkutsk 650033, Russia

* Corresponding author: kovtunets@binm.ru



Abstract

A new glaserite-like ternary molybdate $\text{KZn}_{0.5}\text{Hf}_{0.5}(\text{MoO}_4)_2$ was obtained through a solid-state reaction, and its structure was refined using the Rietveld method. It was found that the compound crystallizes in the trigonal space group $P\bar{3}m1$ and melts at 656 °C with decomposition. At elevated temperatures, the compound exhibited significant ionic conductivity, reaching $0.39 \cdot 10^{-3}$ S/cm at 570 °C with an activation energy $E_a = 1.0$ eV, with oxygen ions as the probable charge carriers. The infrared spectrum simulated using DFT showed good agreement with experimental data, containing characteristic stretching modes of the MoO_4 tetrahedra. The observed negative thermal expansion in the *ab* plane did not result in a reduction in the volume of the unit cell, with $\alpha_v = 98 \cdot 10^{-6}$ °C⁻¹ at 500 °C, indicating that $\text{KZn}_{0.5}\text{Hf}_{0.5}(\text{MoO}_4)_2$ can be classified as a material with high thermal expansion properties.

Key findings

- Ionic conductivity reaches $0.39 \cdot 10^{-3}$ S/cm at 570 °C with $E_a = 1.0$ eV. O^{2-} ions are probable charge carriers.
- IR spectrum simulated by DFT showed good agreement with experimental data.
- The observed 2D-NTE effect does not lead to a decrease in the unit cell volume.

© 2024, the Authors. This article is published in open access under the terms and conditions of the Creative Commons Attribution (CC BY) license (<http://creativecommons.org/licenses/by/4.0/>).

1. Introduction

The development of new functional materials largely depends on the systematic study of multicomponent oxide systems, along with the processes of forming new compounds, and the determination of their structural and physicochemical characteristics. Complex molybdates identified through this approach, characterized by a diverse cationic composition, often exhibit unique physical properties and have extensive applications as piezoelectric and ferroelectric materials [1, 2], phosphors [3–7], solid electrolytes [8–11], and other types of materials [12–15].

Earlier, the first representatives of new structural families $\text{K}_5\text{Mg}_{0.5}\text{Zr}_{1.5}(\text{MoO}_4)_6$ and $\text{KMg}_{0.5}\text{Zr}_{0.5}(\text{MoO}_4)_2$ were obtained through the study of the potassium-containing system $\text{K}_2\text{MoO}_4\text{--MgMoO}_4\text{--Zr}(\text{MoO}_4)_2$ [16, 17]. The family of

ternary molybdates with a framework structure KMZ, which originated from the compound $\text{K}_5\text{Mg}_{0.5}\text{Zr}_{1.5}(\text{MoO}_4)_6$ (space group $R3c$), includes a large number of representatives. The relationships between the composition, structure, and functional properties of these compounds are currently the subject of extensive studies [18–21].

In contrast to the trigonal ternary molybdate $\text{K}_5\text{Mg}_{0.5}\text{Zr}_{1.5}(\text{MoO}_4)_6$ with a framework structure, the compound $\text{K}(\text{Mg}_{0.5}\text{Zr}_{0.5})(\text{MoO}_4)_2$ (space group $P\bar{3}m1$) crystallizes in the structural type of trigonal glaserite [17], which is widely spread among silicates, phosphates, sulfates, molybdates, and tungstates [22]. This type features a two-layer compact arrangement of MoO_4 tetrahedra, which is analogous to the hexagonal closest packing. The octahedral cavities formed by the faces of the MoO_4 tetrahedra are occupied by divalent and tetravalent cations Mg^{2+} and Hf^{4+} .

Accompanying information

Article history

Received: 28.11.24

Revised: 24.01.25

Accepted: 24.01.25

Available online: 28.01.25


Keywords

ternary molybdate, thermal expansion, conductivity, solid-phase synthesis, structure, high-temperature X-ray diffraction

Funding

This work was supported by the Russian Science Foundation (grant no. [23-29-00327](#)).

Supplementary information

Supplementary materials: 

Transparent peer review: 

Sustainable Development Goals



The interlayer space is filled with potassium cations K^+ . An interesting feature of this structure is the orientation of one of the triangular faces of each MoO_4 tetrahedron parallel to the layer plane, which creates a two-dimensional infinite network consisting of O^{2-} ions, potentially facilitating oxygen migration [23]. Ceramic materials based on compounds belonging to the glaserite-type are promising as matrices for the development of phosphors, as dopants (transition metal impurities) under the influence of a unique crystal-chemical environment exhibit intense visible emission [24].

This work presents the results of the targeted synthesis and study of the properties of a new representative of the little-studied and scarce glaserite-like family of ternary molybdates – $KZn_{0.5}Hf_{0.5}(MoO_4)_2$. The structure of the polycrystalline sample was refined using the Rietveld method, and its thermal properties and ionic conductivity were investigated.

2. Experimental

The following starting reagents were used for solid state reactions: K_2MoO_4 (chemically pure, RusHim, Ltd, Russia), ZnO (chemically pure, LenReactiv, Ltd, Russia), HfO_2 (high purity, Sigma-Aldrich, China), and MoO_3 (analytical grade, ReaKhim, Ltd, Russia). Ternary molybdate $K(Zn_{0.5}Hf_{0.5})(MoO_4)_2$ was synthesized from a stoichiometric mixture of K_2MoO_4 , $ZnMoO_4$ and $Hf(MoO_4)_2$ molybdates. Zinc molybdate $ZnMoO_4$ and hafnium molybdate $Hf(MoO_4)_2$ were synthesized by stepwise annealing of stoichiometric mixtures of the corresponding oxides in the temperature ranges of 350–650 °C and 350–750 °C, respectively, over a 100-hour period. During the synthesis, the samples were regularly ground in ethanol.

The solid-state synthesis and phase equilibrium were monitored by XRD using a Bruker D8 ADVANCE diffractometer (VANTEC detector, $Cu\ K\alpha$ radiation, $\lambda = 1.5418\ \text{\AA}$, reflection geometry). The XRD data were collected at room temperature in the 2θ range of 10–100° with a step size of 0.02076°. High-temperature powder X-ray diffraction (HT-PXRD) measurements were conducted using an Anton Paar HTK16 high-temperature chamber, in the temperature range of 30–600 °C, with 50 °C increments. For the measurements, a finely ground sample was applied to a platinum sample holder using an ethanol suspension. Prior to the measurements, the 2θ -correction was recorded using an external Si standard. Structure refinement and unit cell parameter calculations were performed using the Rietveld method with the TOPAS 4.2 software [25]. The visualization and calculation of the thermal expansion tensor parameters were carried out using the TTT software package [26].

Thermogravimetric (TG) and differential scanning calorimetry (DSC) studies were conducted in a platinum crucible under an argon flow using an STA 449 F1 Jupiter NETZSCH thermoanalyzer within the temperature range of 30–700 °C at a heating rate of 10 °C /min.

The theoretical assessment of activation energy and ion transport pathways in the title molybdate was performed using the softBV software [27], employing bond valence sum (BVS) maps.

Electrical conductivity measurements were performed in a temperature range of 100–570 °C using a Z-1500J impedance analyzer under heating and cooling modes (2°/min) across a frequency range of 1 Hz to 1 MHz. To investigate ionic conductivity, ceramic discs of $KZn_{0.5}Hf_{0.5}(MoO_4)_2$ with a diameter of 10 mm and a thickness of 1.9 mm were prepared by pressing (1 kbar) and sintering at 570 °C for 4 h. Electrodes were applied to the surface of the discs using colloidal platinum, followed by annealing for 1 h.

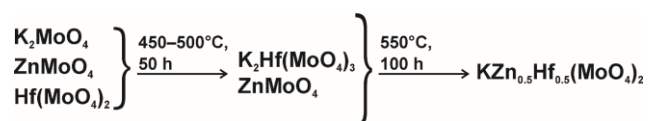
Attenuated total reflectance infrared spectra (ATR-IR) of $KZn_{0.5}Hf_{0.5}(MoO_4)_2$ were recorded using a SIMEX FT-801 FT-IR spectrometer with a diamond ATR cell. The spectra were collected at room temperature in the range from 500 to 2000 cm^{-1} with a resolution of 1 cm^{-1} .

To simulate the IR spectrum, the geometry of the crystal structure of $KZn_{0.5}Hf_{0.5}(MoO_4)_2$ was optimized using density functional theory (DFT) within the VASP software package [28]. The calculations utilized a pseudopotential approach along with plane-wave basis sets, with the cutoff energy established at 400 eV. The PBEsol functional was chosen to approximate the exchange-correlation term in the Hamiltonian [29]. A Gamma-centered 1·1·1 k-point mesh was employed for sampling the Brillouin zone. The initial geometry was derived from the crystal structure model obtained from the XRD data. Atomic positions were relaxed until the residual forces on the atoms were reduced to less than 0.001 eV/Å, while the lattice vectors were held fixed at their experimental values. Phonon calculations were carried out using the results from VASP and the methods implemented in the Phonopy code [30]. The IR spectra were then simulated with the Phonopy-Spectroscopy code [31].

3. Results and discussion

3.1. Solid-state synthesis of $KZn_{0.5}Hf_{0.5}(MoO_4)_2$

Molybdate $KZn_{0.5}Hf_{0.5}(MoO_4)_2$ was synthesized via ceramic technology in an alumina crucible (Al_2O_3 99.7%, PodolskOgneUpor, Russia) through stepwise annealing in the temperature range of 400–550 °C over a 150-hour period. According to XRD data, the sequence of transformations can be represented by the following Scheme 1. Thus, it was found that the formation of the ternary molybdate proceeded through the intermediate stage of forming the potassium-hafnium binary molybdate, $K_2Hf(MoO_4)_3$.



Scheme 1 Sequence of chemical transformations involved in the formation of $KZn_{0.5}Hf_{0.5}(MoO_4)_2$.

3.2. Rietveld refinement and glaserite-like structure of $\text{KZn}_{0.5}\text{Hf}_{0.5}(\text{MoO}_4)_2$

All XRD peaks of $\text{KZn}_{0.5}\text{Hf}_{0.5}(\text{MoO}_4)_2$ could be indexed in a trigonal unit cell (space group $P\bar{3}m1$) with lattice parameters close to those of $\text{K}(\text{Mg}_{0.5}\text{Zr}_{0.5})(\text{MoO}_4)_2$ [17]. The structural data of the latter compound (unit cell parameters and atomic positions) were used as the starting model for structure refinement via the Rietveld method. The peak shapes were described using the Pearson VII function with a correction for sample texture along the 001 direction applied using the March-Dollase function. The refinement was carried out by gradually introducing refinable parameters, while the background was simultaneously modeled graphically.

The final refinement was stable with low residual R-factors. The results obtained for $\text{KZn}_{0.5}\text{Hf}_{0.5}(\text{MoO}_4)_2$ are presented in Table 1, the main interatomic distances are given in Table S1, and the atomic coordinates and isotropic displacement parameters – in Table S2.

The calculated and experimental XRD patterns along with the difference curve are illustrated in Figure 1. The crystallographic data for $\text{KZn}_{0.5}\text{Hf}_{0.5}(\text{MoO}_4)_2$ were deposited with the Cambridge Crystallographic Data Centre (CSD 2392315). The data are available on the website (www.ccdc.cam.ac.uk/data_request/cif).

$\text{KZn}_{0.5}\text{Hf}_{0.5}(\text{MoO}_4)_2$ crystallizes in a trigonal system, space group $P\bar{3}m1$, and has the trigonal glaserite-type structure [17]. The structure is composed of alternating layers with varying compositions, arranged perpendicular to the c -axis. The layer composed of $(\text{Zn}/\text{Hf})\text{O}_6$ octahedra is connected to the layer of KO_{12} icosahedra through shared edges of MoO_4 tetrahedra. The Mo atoms are located on a three-fold rotation axis 3, while the Zn, Hf, and K atoms – on a threefold inversion axis $\bar{3}$ (Figure 2).

3.3. FTIR (IR spectra)

The IR spectra of the investigated compound were analyzed to clarify the coordination of molybdenum atoms. The spectra of the molybdate display bands corresponding to the internal vibrations of MoO_4 groups, with frequencies in the range of $980\text{--}700\text{ cm}^{-1}$ (stretching vibrations) and $410\text{--}300\text{ cm}^{-1}$ (deformation vibrations). The presence of these bands is consistent with the existence of separate tetrahedral groupings with relatively strong Mo–O [32]. A comparison of the measured wavenumbers corresponding to the framework vibrations with the theoretical values resulting from the DFT calculations is given in Table 4. The range of the experimental IR spectra covers only the stretching modes of MoO_4 tetrahedra.

A comparison of the simulated and measured IR spectra of $\text{KZn}_{0.5}\text{Hf}_{0.5}(\text{MoO}_4)_2$ is shown in Figure 3. The positions of the bands in both the simulated and experimental spectra are in agreement (including in the $700\text{--}980\text{ cm}^{-1}$ range), although some differences in their intensities are observed (Table S3).

Table 1 Main parameters of processing and refinement of the $\text{KZn}_{0.5}\text{Hf}_{0.5}(\text{MoO}_4)_2$ sample.

Compound	$\text{KZn}_{0.5}\text{Hf}_{0.5}(\text{MoO}_4)_2$
Space group	Trigonal, $P\bar{3}m1$
a , Å	5.76743 (7)
c , Å	7.17193 (9)
V , Å ³	206.60 (1)
Z	1
2θ -range, °	10–100
R_{wp} , %	6.81
R_p , %	5.38
R_{exp} , %	3.97
χ^2	1.72
R_B , %	4.16

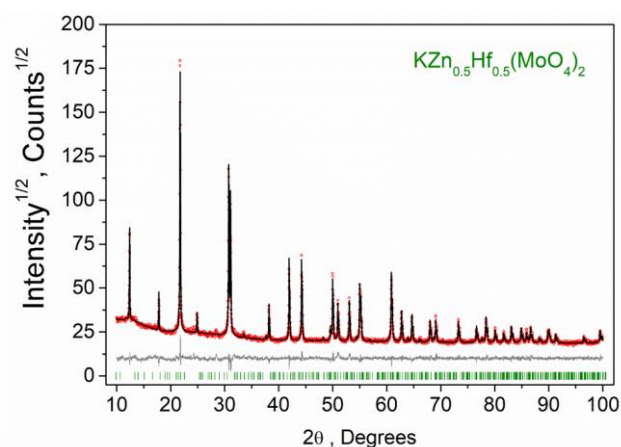


Figure 1 Difference Rietveld plot of $\text{KZn}_{0.5}\text{Hf}_{0.5}(\text{MoO}_4)_2$.

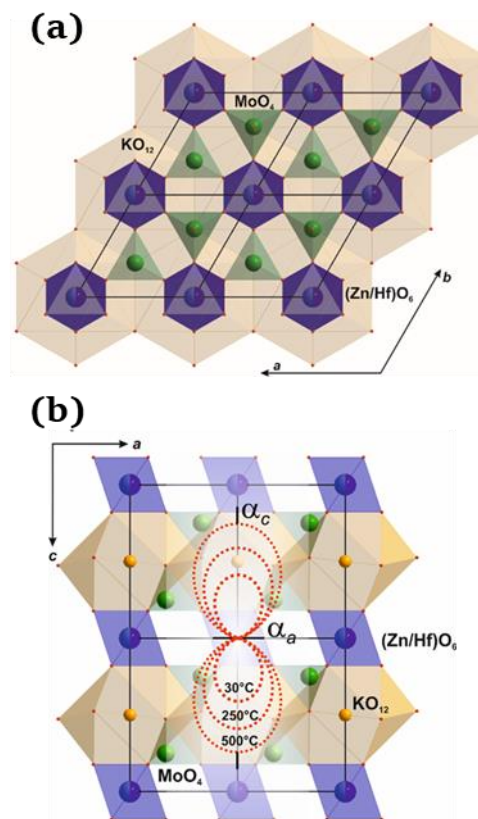


Figure 2 Projection of the $\text{KZn}_{0.5}\text{Hf}_{0.5}(\text{MoO}_4)_2$ structure on the ab plane (a); and ac plane, mapped to the thermal expansion tensor cross-section (b).

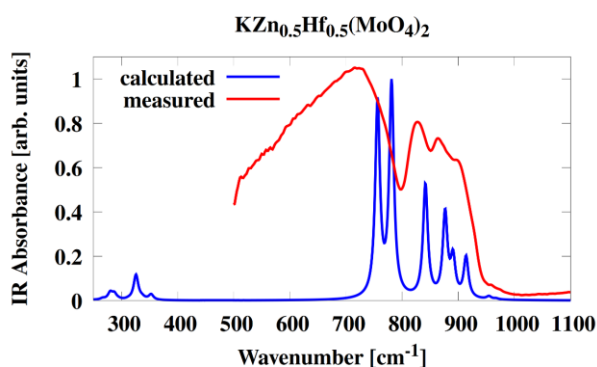


Figure 3 Simulated and experimental IR spectra of $\text{KZn}_{0.5}\text{Hf}_{0.5}(\text{MoO}_4)_2$.

3.4. Thermal properties

The thermal behavior of $\text{KZn}_{0.5}\text{Hf}_{0.5}(\text{MoO}_4)_2$ was investigated using TG and DSC methods. As shown in Figure 4, the DSC curve exhibited a sharp endothermic peak starting at 650 °C along with a lower intensity peak in the 532–544 °C range. The distinct endothermic effect in the 650–660 °C range corresponded to melting. No weight loss was observed on the TG curve. The Rietveld-refined XRD patterns of $\text{KZn}_{0.5}\text{Hf}_{0.5}(\text{MoO}_4)_2$ after annealing at 700 °C and 800 °C indicated partial decomposition of the compound, resulting in the formation of ZnMoO_4 , $\text{K}_2\text{Mo}_3\text{O}_{10}$, $\text{K}_2\text{Zn}_2(\text{MoO}_4)_3$, and HfO_2 .

To ascertain the nature of the endothermic effect observed at 538 °C, the $\text{KZn}_{0.5}\text{Hf}_{0.5}(\text{MoO}_4)_2$ sample was further analyzed in a ‘heating-cooling’ mode within the temperature range of 450–550 °C (below the melting point). Upon cooling, an exothermic effect was detected at 525 °C. The observed thermal hysteresis of 13 °C indicated the presence of a reversible phase transition (Type I) within the 532–544 °C range.

All reflections on the HT diffraction patterns in the entire studied temperature range are indexed in the same space group $P\bar{3}m1$. As an example, Figure S1 shows the refinement of the structure at 600 °C (the coordinates of the atoms were not refined). As can be seen, no new peaks were detected. This indicates that the first-order phase transition is not accompanied by a change in the structure.

3.5. Thermal expansion of $\text{KZn}_{0.5}\text{Hf}_{0.5}(\text{MoO}_4)_2$

The refinement of the unit cell parameters of $\text{KZn}_{0.5}\text{Hf}_{0.5}(\text{MoO}_4)_2$ showed that as the temperature increased from 30 to 600 °C, the value of parameter *a* decreased from 5.7616(2) Å to 5.7508(2) Å (–0.19%), indicating negative thermal expansion in the *ab* plane. Similar 2D negative thermal expansion was observed for some compounds [33], but it is not typical of previously studied glaserite-like structures [34]. Meanwhile, the *c* parameter increased from 7.1665(2) Å to 7.5306(2) Å (+5.08%), demonstrating positive thermal expansion (Figure 5 and Table S4).

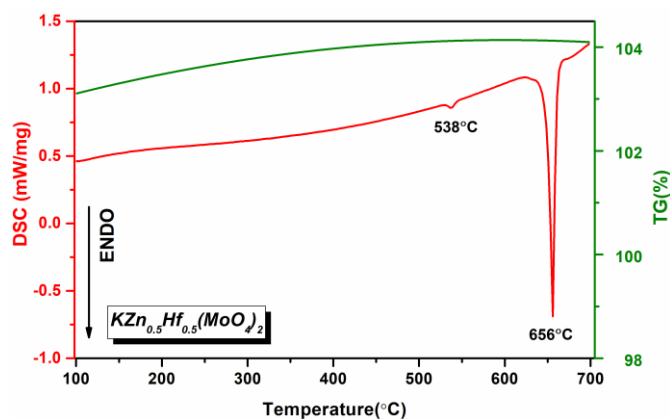


Figure 4 Heating curve of DSC and TG of $\text{KZn}_{0.5}\text{Hf}_{0.5}(\text{MoO}_4)_2$.

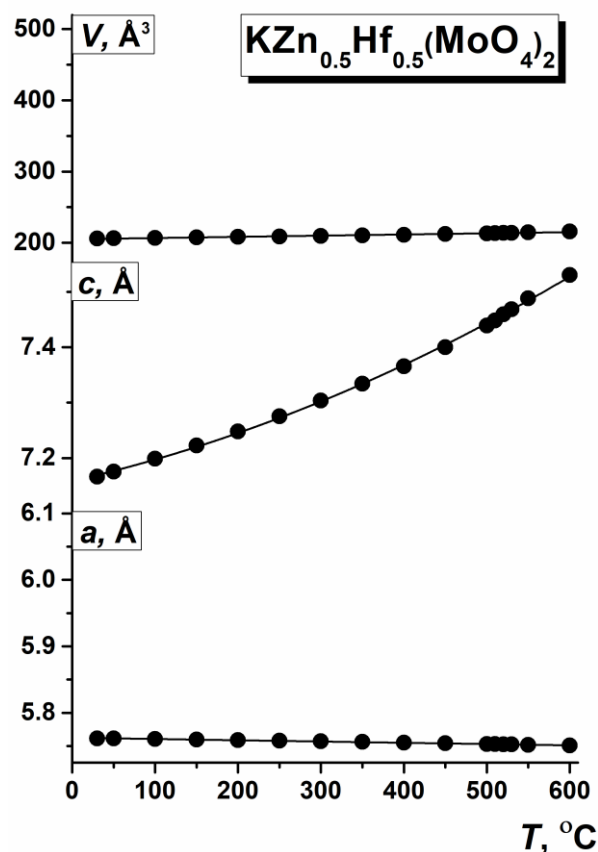


Figure 5 Temperature dependencies of the unit cell parameters.

The temperature dependences of the unit cell parameters were approximated using first-order polynomials (for *a* and *V*) and second-order polynomial (for *c*) (Table S5). A slight inflection was observed on the temperature dependence curve of the *c* parameter around 530 °C (which corresponds to the DSC data) followed by a more pronounced increase in this parameter. Based on the obtained data, the principal values of the thermal expansion tensor were calculated (Table 2), and cross-sections of the thermal expansion coefficient were plotted (Figure 2b).

The coefficient of thermal expansion (CTE) α_c varied between $55 \cdot 10^{-6} \text{ °C}^{-1}$ and $114 \cdot 10^{-6} \text{ °C}^{-1}$ throughout the investigated temperature range, while α_a remained negative at $-3.3 \cdot 10^{-6} \text{ °C}^{-1}$.

Table 2 Thermal expansion coefficients ($\cdot 10^{-6} \text{ }^\circ\text{C}^{-1}$).

$T, ^\circ\text{C}$	α_a	α_c	α_v
30	-3.3(1)	55(2)	49(2)
50	-3.3(1)	58(1)	51(2)
100	-3.3(1)	63(1)	56(2)
150	-3.3(1)	68(1)	62(2)
200	-3.3(1)	74(1)	67(2)
250	-3.3(1)	79(1)	73(2)
300	-3.3(1)	84(1)	78(2)
350	-3.3(1)	90(1)	83(2)
400	-3.3(1)	95(1)	88(2)
450	-3.3(1)	100(1)	93(2)
500	-3.3(1)	105(1)	98(2)
510	-3.3(1)	106(1)	99(2)
520	-3.3(1)	107(1)	100(2)
530	-3.3(1)	108(1)	101(2)
550	-3.3(1)	110(2)	103(2)
600	-3.3(1)	114(2)	108(2)

Despite this, no reduction in cell volume was observed. The values of α_v for $\text{KZn}_{0.5}\text{Hf}_{0.5}(\text{MoO}_4)_2$ were $49 \cdot 10^{-6} \text{ }^\circ\text{C}^{-1}$ at room temperature and $98 \cdot 10^{-6} \text{ }^\circ\text{C}^{-1}$ at 500 $^\circ\text{C}$.

Synchronous change of two unit cell parameters a and c in opposite directions is a sign of the hinge mechanism [35, 36] of thermal deformations [37]. Figure S2 shows a scheme of a complex three-dimensional hinge with nodes at the points $\{\text{Mo-O}_2\text{-(Zn/Hf)-O}_2\text{-Mo-O}_2\text{-(Zn/Hf)-O}_2\}_\infty$. The basic element of this complex hinge structure is the Mo-O₂-(Zn/Hf) hinge. Squeezing the hinge in the ab plane will lead to its extension in the direction of the c axis and vice versa. The reasons for such thermal behavior are the symmetry constrains imposed on the possible displacements of atoms upon heating. Given that the Hf, Zn, K, Mo, and O1 atoms occupy special Wyckoff positions 1a, 1a, 1b, 2d, and 2d, respectively, their movements during heating or cooling cannot cause changes in the unit cell parameters within the ab plane. The negative thermal expansion in the ab plane is likely attributable to the thermal motion of the oxygen atom O2 (Wyckoff position 6i), as it is the only atom with the necessary degree of freedom. The expansion of the unit cell along the crystallographic c -axis can be attributed to the movement of the Mo, O1, and O2 atoms along this axis.

Given that the Hf, Zn, K, Mo, and O1 atoms occupy special Wyckoff positions 1a, 1a, 1b, 2d, and 2d, respectively, their movements during heating or cooling cannot cause changes in the unit cell parameters within the ab plane. The negative thermal expansion in the ab plane is likely attributable to the thermal motion of the oxygen atom O2 (Wyckoff position 6i), as it is the only atom with the necessary degree of freedom. The expansion of the unit cell along the crystallographic c -axis can be attributed to the movement of the Mo, O1, and O2 atoms along this axis.

3.6. Electrical conductivity and the theoretical evaluation of activation energy and ion transport pathways

The electrophysical properties of the examined ternary molybdate were also characterized. The temperature dependence of conductivity (in a heating-cooling cycle) at various frequencies is presented in Figure 6. The impedance plots, which are typical for ionic conductors with blocking electrodes, are shown in Figure 7.

Conductivity monotonically increased with rising temperature (100–500 $^\circ\text{C}$) from 10^{-9} to 10^{-6} S/cm. A subsequent sharp increase in conductivity was observed, reaching a value of $0.39 \cdot 10^{-3}$ S/cm (570 $^\circ\text{C}$) with an activation energy $E_a = 1.0$ eV. During heating and cooling (at 530 $^\circ\text{C}$ and 520 $^\circ\text{C}$, respectively), a change in the linearity of the temperature dependence of conductivity was observed (Figure 6). These values correlated with the temperature of the endothermic effect detected in the DSC curve (Figure 4), indicating a first-order phase transition, which was further confirmed by the presence of thermal hysteresis (Figure 6).

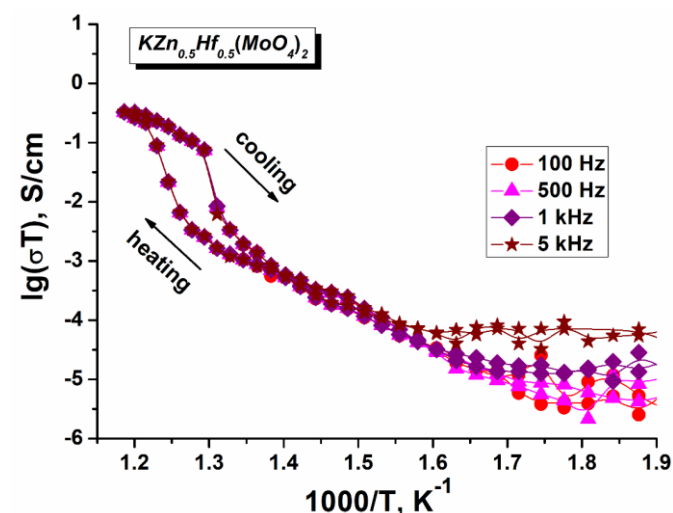


Figure 6 Temperature dependences of electrical conductivity for $\text{KZn}_{0.5}\text{Hf}_{0.5}(\text{MoO}_4)_2$.

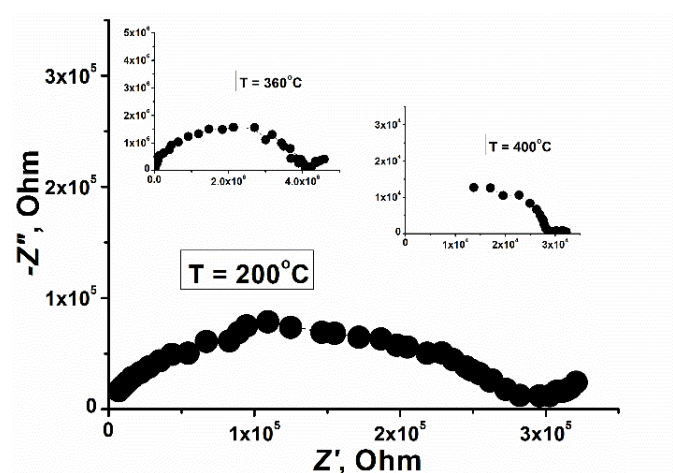


Figure 7 The impedance profiles for $\text{KZn}_{0.5}\text{Hf}_{0.5}(\text{MoO}_4)_2$ measured at different temperatures.

The pattern of the temperature dependence of conductivity is similar to that of the isostructural molybdate $\text{KMg}_{0.5}\text{Zr}_{0.5}(\text{MoO}_4)_2$ [23]. Conductivity values for compounds within this family are presented in Table S6. These values are comparable, likely due to the relatively close ionic radii of the elements constituting the ternary molybdates (for six-coordinate cations, the ionic radii are: 0.72 (Mg^{2+}), 0.74 (Zn^{2+}), 0.71 (Hf^{4+}), and 0.72 (Zr^{4+}) Å [38]). We propose that the larger ionic radius of manganese (0.83 Å) may contribute to an increase in interlayer spacing within the structure of $\text{KMn}_{0.5}\text{Zr}_{0.5}(\text{MoO}_4)_2$ [39], providing more space for ionic transport.

Using the structural data for $\text{KZn}_{0.5}\text{Hf}_{0.5}(\text{MoO}_4)_2$, bond valence sum (BVS) maps were calculated for potassium and oxygen ions (the most likely charge carriers), and possible diffusion pathways for these ions were predicted. The calculations indicated a predominance of two-dimensional oxygen conductivity (Figure 8) and suggested the impossibility of potassium movement within the examined structure. For comparison, analogous calculations for the isostructural zirconium molybdate are presented in Table 3.

In both $\text{KZn}_{0.5}\text{Hf}_{0.5}(\text{MoO}_4)_2$ and its zirconium analogue, the two-dimensional diffusion pathways of oxygen ions involve the oxygen ions O2 of the molybdenum tetrahedra in the (0,0,1) plane (Figure 9).

4. Limitation

To gain better interpretation of electrical conductivity, the experimental verification of the theoretical calculations results of oxygen conductivity will be done in the future.

5. Conclusions

Ternary molybdate $\text{KZn}_{0.5}\text{Hf}_{0.5}(\text{MoO}_4)_2$ was synthesized via a solid-state reaction. Its structure was refined using the Rietveld method, taking the crystallographic data from the single crystal sample $\text{KMg}_{0.5}\text{Zr}_{0.5}(\text{MoO}_4)_2$ [17] as starting parameters. The title compound crystallizes in the trigonal space group $P\bar{3}m1$. Differential scanning calorimetry (DSC) and thermogravimetric analysis (TG) results demonstrated that $\text{KZn}_{0.5}\text{Hf}_{0.5}(\text{MoO}_4)_2$ melted at 656 °C with decomposition.

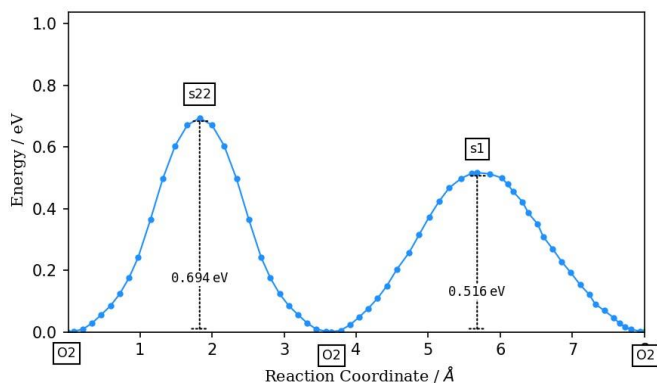


Figure 8 Energy profile along the 2D oxygen transport pathway in the structure $\text{KZn}_{0.5}\text{Hf}_{0.5}(\text{MoO}_4)_2$.

Table 3 Energy barriers E_b (eV) of two- and three-dimensional oxygen transport in $\text{KA}_{0.5}\text{R}_{0.5}(\text{MoO}_4)_2$.

Compound	E_b	Dimension of conductivity
$\text{KMg}_{0.5}\text{Zr}_{0.5}(\text{MoO}_4)_2$ [23]	0.685	2D along (0,0,1)
	1.166	3D
$\text{KZn}_{0.5}\text{Hf}_{0.5}(\text{MoO}_4)_2$	0.694	2D along (0,0,1)
	0.993	3D

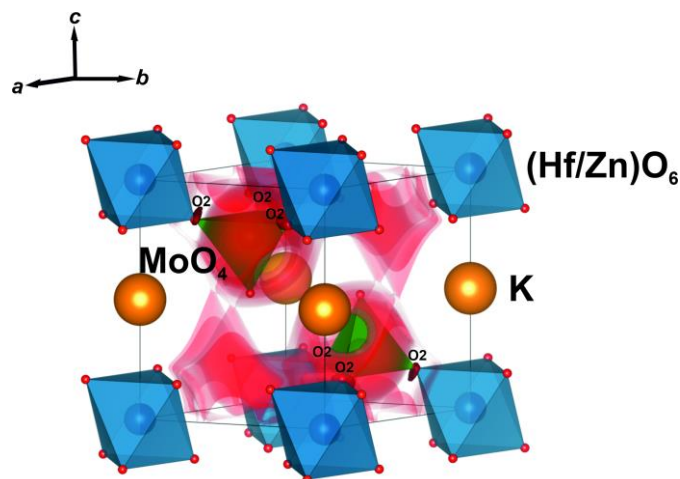


Figure 9 Calculated isosurfaces of activation energies of oxygen transport in the structure $\text{KZn}_{0.5}\text{Hf}_{0.5}(\text{MoO}_4)_2$.

In this study we also investigated the ionic conductivity properties of $\text{KZn}_{0.5}\text{Hf}_{0.5}(\text{MoO}_4)_2$, which reached a conductivity value of $0.39 \cdot 10^{-3}$ S/cm at 570 °C with an activation energy $E_a = 1.0$ eV. Theoretical assessment of the transport energy barriers in $\text{KZn}_{0.5}\text{Hf}_{0.5}(\text{MoO}_4)_2$, based on bond valence sum (BVS) maps, revealed that the structure primarily facilitates two-dimensional oxygen conductivity with no identified pathways for potassium ion movement.

The assignment of framework vibration bands in the IR spectrum of $\text{KZn}_{0.5}\text{Hf}_{0.5}(\text{MoO}_4)_2$ was performed using DFT calculations. The simulated IR spectrum showed good agreement with the experimental data, containing characteristic lines of the stretching modes of MoO_4 tetrahedra, thus confirming the coordination of Mo atoms in the refined structure.

Thermal deformations of $\text{KZn}_{0.5}\text{Hf}_{0.5}(\text{MoO}_4)_2$ were investigated using HT-XRD. The observed negative thermal expansion in the ab plane did not lead to a reduction in the cell volume. The value of α_V for $\text{KZn}_{0.5}\text{Hf}_{0.5}(\text{MoO}_4)_2$ to be $98 \cdot 10^{-6}$ °C⁻¹ at 500 °C, which categorizes this phase as a material with high thermal expansion properties.

Supplementary materials

This manuscript contains supplementary materials, which are available on the corresponding online page.

Data availability statement

The data that support the findings of this study are available from the corresponding author upon reasonable request.

Acknowledgments

The X-ray phase analysis, high-temperature X-ray diffraction, infrared spectroscopy, and conductivity measurements were carried out using the resources of the Research Equipment Sharing Center

of BINM SB RAS (Ulan-Ude, Russia). Ab initio calculations were performed on “Academician V.M. Matrosov” facilities of Irkutsk Supercomputer Center SB RAS (<https://hpc.icc.ru>).

Author contributions

Conceptualization: E.K., B.B.
 Data curation: A.L., Y.T., T.B.
 Formal Analysis: E.K., T.S., Y.T., B.B.
 Funding acquisition: B.B.
 Investigation: E.K., T.S., Y.T., T.B., A.L., A.B.
 Methodology: E.K., T.S., Y.T.
 Project administration: B.B.
 Resources: B.B., A.B.
 Software: E.K., T.S., A.B.
 Supervision: B.B.
 Validation: E.K., T.S., B.B., Y.T.
 Visualization: E.K., T.S.
 Writing – original draft: E.K., T.S.
 Writing – review & editing: E.K., T.S., B.B., Y.T.

Conflict of interest

The authors declare no conflict of interest.

Additional information

Author IDs:

Evgeniy Kovtunets, Scopus ID [57216460806](https://orcid.org/0000-0001-5721-6460);
 Yunna Tushinova, Scopus ID [6507295454](https://orcid.org/0000-0001-6507-2954);
 Tatyana Spiridonova, Scopus ID [57198791455](https://orcid.org/0000-0001-5719-8791);
 Tsyrendyshit Bazarova, Scopus ID [6603469765](https://orcid.org/0000-0001-6603-4697);
 Alexandra Logvinova, Scopus ID [57197825558](https://orcid.org/0000-0001-5719-7825);
 Alexandr Bogdanov, Scopus ID [57191578487](https://orcid.org/0000-0001-5719-1578);
 Bair Bazarov, Scopus ID [70047455799](https://orcid.org/0000-0001-7004-7455).

Websites:

Baikal Institute of Nature Management, <https://www.binm.ru/>;
 Institute of Geochemistry, <http://igc.irk.ru/ru/>;
 Irkutsk Supercomputer Center, <https://hpc.icc.ru/>.

References

1. Tsyrenova GD, Pavlova ET, Solodovnikov SF, Popova NN, Kardash TY, Stefanovich SY, Gudkova IA, Solodovnikova ZA, Lazoryak BI. New ferroelastic $K_2Sr(MoO_4)_2$: synthesis, phase transitions, crystal and domain structures, ionic conductivity. *J Solid State Chem.* 2016;237:64–71. doi:[10.1016/j.jssc.2016.01.011](https://doi.org/10.1016/j.jssc.2016.01.011)
2. Ben NW, Ben RA. Ferroelectric properties and alternative current conduction mechanisms of lithium rubidium molybdate. *Ionics.* 2019;25:4003–4012. doi:[10.1007/s11581-019-02921-w](https://doi.org/10.1007/s11581-019-02921-w)
3. Stefańska D, Kabański A, Adaszyński M, Ptak M, Lisiecki R, Starościk N, Hanuza J. Broadband near-infrared luminescence properties of $Sc_2(MoO_4)_3:Cr^{3+}$ molybdates. *Spectrochim. Acta Mol Biomol Spectrosc.* 2023;296:122699. doi:[10.1016/j.saa.2023.122699](https://doi.org/10.1016/j.saa.2023.122699)
4. Ren H, Li H, Zou Y, Deng H, Peng Z, Ma T, Ding S. Growth and properties of Pr^{3+} -doped $NaGd(MoO_4)_2$ single crystal: a promising InGaN laser-diode pumped orange-red laser crystal. *J Lumin.* 2022;249:119034. doi:[10.1016/j.jlumin.2022.119034](https://doi.org/10.1016/j.jlumin.2022.119034)
5. Wang J, Luo L, Huang B, He J, Zhang W, Zhao W, Wang J. The preparation and optical properties of novel $LiLa(MoO_4)_2:Sm^{3+},Eu^{3+}$ red phosphor. *Mater.* 2018;11(2):297. doi:[10.3390/ma11020297](https://doi.org/10.3390/ma11020297)
6. Spassky D, Vasil'ev A, Jamal MU, Morozov VA, Lazoryak BI, Redkin BS, Chernenko K, Nagirnyi V. Temperature dependent energy transfer to Eu^{3+} emission centres in $K_5Eu(MoO_4)_4$ crystals. *CrystEngComm.* 2024;26(8):1106–1116. doi:[10.1039/D3CE01201H](https://doi.org/10.1039/D3CE01201H)
7. Posokhova SM, Morozov VA, Zonov EM, Deyneko DV, Spassky DA, Fedyunin FD, Belik AA, Pavlova ET, Vasing AA, Lazoryak BI. $K_5Yb_{1-x}Eu_x(MoO_4)_4$ phosphors: aperiodic structures and luminescence properties. *CrystEngComm.* 2023;25:4822–4833. doi:[10.1039/D3CE00401E](https://doi.org/10.1039/D3CE00401E)
8. Solodovnikov SF, Gulyaeva OA, Savina AA, Yudin VN, Buzlukov AL, Solodovnikova ZA, Zolotova ES, Spiridonova TS, Khaikina EG, Stefanovich SY, Medvedeva NI, Baklanova YV, Denisova TA. Molybdates and tungstates of the alluaudite family: crystal chemistry, composition, and ionic mobility. *J Struct Chem.* 2022;63:1101–1133. doi:[10.1134/S0022476622070071](https://doi.org/10.1134/S0022476622070071)
9. Buzlukov AL, Fedorov DS, Serdtsev AV, Kotova IY, Tyutyunnik AP, Korona DV, Baklanova YV, Ogloblichev VV, Kozhevnikova NM, Denisova TA, Medvedeva NI. Ion mobility in triple sodium molybdates and tungstates with a NASICON structure. *J Exp Theor Phys.* 2022;134:42–50. doi:[10.1134/S1063776122010071](https://doi.org/10.1134/S1063776122010071)
10. Grossmana VG, Molokeyev MS, Bazarov BG, Bazarova JG. Potassium and thallium conductors with a trigonal structure in the $M_2MoO_4-Cr_2(MoO_4)_3-Hf(MoO_4)_2$ (M = K, Tl) systems: Synthesis, structure, and ionic conductivity. *J Alloys Compd.* 2021;873:159828. doi:[10.1016/j.jallcom.2021.159828](https://doi.org/10.1016/j.jallcom.2021.159828)
11. Spiridonova TS, Solodovnikov SF, Savina AA, Kadyrova YM, Solodovnikova ZA, Yudin VN, Stefanovich SY, Khaikina EG. New triple molybdate $Rb_2AgIn(MoO_4)_3$: synthesis, framework crystal structure and ion transport behavior. *Acta Crystallogr. C.* 2018;74:1603–1609. doi:[10.1107/S2053229618014717](https://doi.org/10.1107/S2053229618014717)
12. Chimitova OD, Bazarov BG, Bazarova JG, Atuchin VV, Azmi V, Sarapulova AE, Mikhailova D, Balachandran G, Fiedler A, Geckle U, Prots Y, Komarek AC, GavriloVA TA, Prosvirin IP, Yang Y, Lin Z, Knapp M, Ehrenberg H. The crystal growth and properties of novel magnetic double molybdate $RbFe_3(MoO_4)_7$ with mixed Fe^{3+}/Fe^{2+} states and 1D negative thermal expansion. *CrystEngComm.* 2021;23:3297–3307. doi:[10.1039/D1CE00118C](https://doi.org/10.1039/D1CE00118C)
13. Nasri R, Larbi T, Amlouk M, Zid MF. Investigation of the physical properties of $K_2Co_2(MoO_4)_3$ for photocatalytic application. *J Mater Sci Mater Electron.* 2018;29:18372–18379. doi:[10.1007/s10854-018-9951-x](https://doi.org/10.1007/s10854-018-9951-x)
14. Alzakree ARH, Wang CH, Shehbaz M, Wang W, Xu D, Du C, Zhou D. Microwave dielectric properties of $(Na_{0.5}Bi_{0.5})MoO_4-BaMoO_4$ composite ceramics with ultralow sintering temperature. *J Am Ceram Soc.* 2024;107(11):7452–7459. doi:[10.1111/jace.20024](https://doi.org/10.1111/jace.20024)
15. Binish B, Durairaj M, Sabari Girisun TC, Mani Rahulan K. Engineering the nonlinear optical properties of barium molybdate by doping Sn^{4+} ions for optical limiting device applications. *Ceram Int.* 2023;49(11):17629–17638. doi:[10.1016/j.ceramint.2023.02.129](https://doi.org/10.1016/j.ceramint.2023.02.129)
16. Klevtsova RF, Bazarova JG, Glinskaya LA, Alekseev VI, Arkhincheeva SI, Bazarov BG, Klevtsov PV, Fedorov KN. Synthesis of ternary potassium, magnesium, and zirconium molybdates. The crystal structure of $K_5(Mg_{0.5}Zr_{1.5})(MoO_4)_6$. *J Struct Chem.* 1994;35:286–290. doi:[10.1007/BF02578278](https://doi.org/10.1007/BF02578278)
17. Klevtsova RF, Bazarova JG, Glinskaya LA, Alekseev VI, Arkhincheeva SI, Bazarov BG, Klevtsov PV. Crystal structure investigation of ternary molybdate $K(Mg_{0.5}Zr_{0.5})(MoO_4)_2$. *J Struct Chem.* 1995;36:809–812. doi:[10.1007/BF02579673](https://doi.org/10.1007/BF02579673)
18. Grossman VG, Molokeyev MS, Bazarova JG, Bazarov BG. High ionic conductivity of $K_{5-x}Tl_x(Mg_{0.5}Hf_{1.5})(MoO_4)_6$ ($0 \leq x \leq 5$) solid solutions. *Solid State Sci.* 2022;134:107027. doi:[10.1016/j.solidstatesciences.2022.107027](https://doi.org/10.1016/j.solidstatesciences.2022.107027)
19. Aksenov SM, Pavlova ET, Popova NN, Tsyrenova GD, Lazoryak BI. Stoichiometry and topological features of triple molybdates $A_xB_yC_z(MoO_4)_n$ with the heteropolyhedral open MT-frameworks: Synthesis, crystal structure of $Rb_5\{Hf_{1.5}Co_{0.5}(MoO_4)_6\}$, and comparative crystal chemistry. *Solid State Sci.* 2024;151:107525. doi:[10.1016/j.solidstatesciences.2024.107525](https://doi.org/10.1016/j.solidstatesciences.2024.107525)
20. E.V. Kovtunets, Yu.L. Tushinova, A.V. Logvinova, Ts.T. Bazarova, B.G. Bazarov. Thermal expansion of ternary molybdate $K_5[Mn_{0.5}Zr_{1.5}](MoO_4)_6$. *ESSUTM Bulletin.* 2024;3(94):90–97. doi:[10.53980/24131997_2024_3_90](https://doi.org/10.53980/24131997_2024_3_90)

21. Kovtunets EV, Spiridonova TS, Tushinova YL, Logvinova AV, Bazarova TT, Bazarov BG. Thermal expansion and ionic conductivity of $K_5Pb_{0.5}Zr_{1.5}(MoO_4)_6$. *Izvestiya Vuzov. Prikladnaya Khimiya i Biotekhnologiya*. 2024;14(4). doi:[10.21285/achb.939](https://doi.org/10.21285/achb.939)
22. Hermanowicz K, Mączka M, Dereń PJ, Hanuza J, Stręk W, Drulis H. Optical properties of chromium(III) in trigonal $KAl(MoO_4)_2$ and monoclinic $NaAl(MoO_4)_2$ hosts. *J Luminescence*. 2000;92(1-2):151-159. doi:[10.1016/S0022-2313\(00\)00232-5](https://doi.org/10.1016/S0022-2313(00)00232-5)
23. Kovtunets E, Tushinova Y, Bazarov B, Bazarova J, Logvinova A, Spiridonova T. A glaserite-like ternary molybdate $K(Mg_{0.5}Zr_{0.5})(MoO_4)_2$: Synthesis, thermal expansion, and ionic conductivity. *Solid State Sci*. 2024;151:107528. doi:[10.1016/j.solidstatesciences.2024.107528](https://doi.org/10.1016/j.solidstatesciences.2024.107528)
24. Brik MG, Avram CN. Exchange charge model and analysis of the microscopic crystal field effects in $KAl(MoO_4)_2 \cdot Cr^{3+}$. *J Luminescence*. 2011;131(12):2642-2645. doi:[10.1016/j.jlumin.2011.06.034](https://doi.org/10.1016/j.jlumin.2011.06.034)
25. Coelho AA. TOPAS and TOPAS-Academic: an optimization program integrating computer algebra and crystallographic objects written in C++. *J Appl Crystallography*. 2018;51:210-218. doi:[10.1107/S1600576718000183](https://doi.org/10.1107/S1600576718000183)
26. Bubnova RS, Firsova VA, Filatov SK. Software for determining the thermal expansion tensor and the graphic representation of its characteristic surface (theta to tensor-TTT). *Glass Phys Chem*. 2013;39:347-350. doi:[10.1134/S108765961303005X](https://doi.org/10.1134/S108765961303005X)
27. Chen H, Wong LL, Adams S. SoftBV - a software tool for screening the materials genome of inorganic fast ion conductors. *Acta Crystallogr Sect B*. 2019;75:18-33. doi:[10.1107/S2052520618015718](https://doi.org/10.1107/S2052520618015718)
28. Gajdoš M, Hummer K, Kresse G, Furthmüller J, Bechstedt F. Linear optical properties in the projector-augmented wave methodology. *Phys Rev*. 2006;73:045112. doi:[10.1103/PhysRevB.73.045112](https://doi.org/10.1103/PhysRevB.73.045112)
29. Perdew JP, Ruzsinszky A, Csonka GI, Vydrov OA, Scuseria GE, Constantin LA, Zhou X, Burke K. Restoring the density-gradient expansion for exchange in solids and surfaces. *Phys Rev Lett*. 2008;100:136406. doi:[10.1103/PhysRevLett.100.136406](https://doi.org/10.1103/PhysRevLett.100.136406)
30. Togo A, Tanaka I. First-principles phonon calculations in materials science. *Scr Mater*. 2015;108:1-5. doi:[10.1016/j.scriptamat.2015.07.021](https://doi.org/10.1016/j.scriptamat.2015.07.021)
31. Skelton JM, Burton LA, Jackson AJ, Oba J, Parker SC, Walsh A. Lattice dynamics of the tin sulphides SnS_2 , SnS and Sn_2S_3 : vibrational spectra and thermal transport. *Phys Chem Chem Phys*. 2017;19:12452-12465. doi:[10.1039/C7CP01680H](https://doi.org/10.1039/C7CP01680H)
32. Fomichev VV, Poloznikova ME, Kondratov OI. Structural features and spectroscopic and energy characteristics of alkali metal molybdates and tungstates. *Russ Chem Rev*. 1992;61(9):877-888. doi:[10.1070/RC1992v061n09ABEH001004](https://doi.org/10.1070/RC1992v061n09ABEH001004)
33. Zhang X, Jiang X, Molokeev MS, Wang N, Liu Y, Lin Zh. Two-dimensional negative thermal expansion in a crystal of $LiBO_2$. *Chem Mater*. 2022;34(9):4195-4201. doi:[10.1021/acs.chemmater.2c00621](https://doi.org/10.1021/acs.chemmater.2c00621)
34. Smith AL, Kauric G, Eijck L, Goubitz K, Clavier N, Wallez G, Konings RJM. Structural and thermodynamic study of $Cs_3Na(MoO_4)_2$: Margin to the safe operation of sodium cooled fast reactors. *J Solid State Chem*. 2019;269:1-8. doi:[10.1016/j.jssc.2018.08.033](https://doi.org/10.1016/j.jssc.2018.08.033)
35. Sleight AW. Thermal Contraction. *Endeavor*. 1995;19(2):64-68. doi:[10.1016/0160-9327\(95\)93586-4](https://doi.org/10.1016/0160-9327(95)93586-4)
36. Sleight AW. Compounds that contract on heating. *Inorg Chem*. 1998;37(12):2854-2860. doi:[10.1021/ic980253h](https://doi.org/10.1021/ic980253h)
37. Filatov SK., Krivovichev SV., Bubnova RS. General crystal chemistry: textbook. St. Petersburg: Publishing house of St. Petersburg University. 2018: 276.
38. Shannon RD. Revised effective ionic radii and systematic studies of interatomic distances in halides and chalcogenides. *Acta Crystallographica*. 1976;32:751-767. doi:[10.1107/S0567739476001551](https://doi.org/10.1107/S0567739476001551)
39. Bazarov BG, Fedorov KN, Bazarova TT, Bazarova JG. Electrical properties of molybdates in the systems M_2MoO_4 - $AMoO_4$ - $Zr(MoO_4)_2$. *Russ J Appl Chem*. 2002;75:1026-1028. doi:[10.1023/A:1020377905907](https://doi.org/10.1023/A:1020377905907)